Journal of Innovative Optical Health Sciences
Vol. 2, No. 2 (2009) 143–147

World Scientific
www.worldscientific.com

NEAR-INFRARED OPTICAL TOMOGRAPHY IMAGE RECONSTRUCTION APPROACH BASED ON TWO-LAYERED BP NEURAL NETWORK

TING LI, WEITAO LI and ZHIYU QIAN*
Department of Biomedical Engineering
Nanjing University of Aeronautics and Astronautics
No. 29 Yudao Street, Nanjing 210016, P. R. China
**zhiyu@nuaa.edu.cn*

An image-reconstruction approach for optical tomography is presented, in which a two-layered BP neural network is used to distinguish the tumor location. The inverse problem is solved as optimization problem by Femlab software and Levenberg–Marquardt algorithm. The concept of the average optical coefficient is proposed in this paper, which is helpful to understand the distribution of the scattering photon from tumor. The reconstructive $\bar{\mu}_s'$ by the trained network is reasonable for showing the changes of photon number transporting inside tumor tissue. It realized the fast reconstruction of tissue optical properties and provided optical OT with a new method.

Keywords: Near-infrared optical tomography; two-layered; back-propagation neural network; inverse problem; the average optical coefficient.

1. Introduction

Near-infrared optical tomography (NIR OT) is a medical-imaging technique in which measurements of near-infrared light transmitted across the body are used to obtain images of tissue with optical properties. It has been emerging as a very promising diagnostic tool in a wide variety of biomedical fields,[1,2] since it has the advantage of relatively cost-effective, and is a simple instrument that offers feasible accuracy without any physical damage to biological tissue. It employs a probing source, which is a near-infrared radiation in the range between 600 and 900 nm.

This technique retrieves the space-dependent distributions of optical properties inside biological tissue by analyzing light intensities measured at boundary surfaces with a well-established optimization scheme. The difference in absorption and/or scattering between the normal and diseased tissues provides the imaging contrast for tissue diagnostics.[3] In past decades, various algorithms[4–6] have been introduced to enhance the NIR OT technique and great efforts have been made to develop more accurate and faster algorithms. However, the development of a reconstruction scheme still remains a challenging problem before it can be used on extensive basis.

A new image-reconstruction algorithm based on two-layered BP (back-propagation) neural network (TLBPNN) to NIR OT is proposed in this paper. TLBPNN can be calculated in parallel, so the scale of calculation can be decreased sharply. Faster and more accurate results can be obtained by this new method.

2. Theory

2.1. *The average optical coefficient*

The path of light transport in the tissue is based on the optical properties, which are absorption coefficient μ_a (cm^{-1}), scattering coefficient μ_s (cm^{-1}), and the anisotropic parameter g. The reduced scattering coefficient can be defined as $\mu_s' = (1-g)\mu_s$ (cm^{-1}). g is always recognized as 0.9 by experience.

The model of the light transporting in the tissue is shown in Fig. 1(a). Because of the different tissue refractive index, the intensity is attenuated when the light goes through the tissue. I_0 is the intensity of line light, I is the intensity of the attenuated light, and x is the scattering distance. In uniform tissue without considering absorption, the definition of μ_s is[7]:

$$I = I_0 e^{-\mu_s x}. \tag{1}$$

Next, we give the definition of average scattering coefficient $\bar{\mu}_s$ (cm^{-1}). When there is a tumor inside the tissue, the intensity of the attenuated light is different from that in the uniform tissue. We can find an average μ_s, as $\bar{\mu}_s$. The model of light transporting in the tissue with tumor is shown in Fig. 1(b). According to the definition of Eq. (1), $\bar{\mu}_s$ is defined as:

$$I = I_0 e^{-\bar{\mu}_s x}. \tag{2}$$

Therefore, according to the same way, we can define the other average optical coefficients, such as $\bar{\mu}_s'$ and $\bar{\mu}_a'$.

2.2. *Photon transport function*

If the tissue medium is high-scattering ($\mu_s \gg \mu_a$), and the light source is isotropic with continuous intensity, photon transport can be described by steady-state Boltzmann equation[8] given by

$$-\nabla \cdot \kappa(r)\nabla\Phi(r) + \mu_a(r)\Phi(r) = q, \tag{3}$$

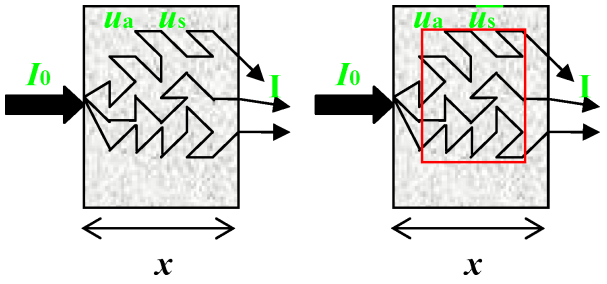

Fig. 1. (a) Scattering attenuation of light through the uniform tissue. (b) Scattering attenuation of light through the tissue with tumor.

where $\Phi(r)$ is the photon density, $\kappa(r) = 1/[3(\mu_a + \mu_s')]$, q is the isotropic light source.

The boundary condition should satisfy the Dirichlet condition $\Phi(boundary) = 0$.

2.3. *Model for average optical coefficient*

The simulated models are shown in Fig. 2. Assume μ_a and μ_s' of the background are $0.01\,\mathrm{cm}^{-1}$ and $5\,\mathrm{cm}^{-1}$ respectively, and μ_a and μ_s' of the tumor region are $0.01\,\mathrm{cm}^{-1}$ and $10\,\mathrm{cm}^{-1}$ respectively. μ_a in the right model is $0.01\,\mathrm{cm}^{-1}$, and μ_s' varies from 5 to $15\,\mathrm{cm}^{-1}$.

After simulation by Femlab software, as shown in Fig. 3, we can get the attenuated photon intensities I_0 and I_1. I_0 is collected from the left model and I_1 is from the right model of Fig. 2. When the error is at the minimum, $\bar{\mu}_s'$ is $5.86\,\mathrm{cm}^{-1}$. It gives the proof of definition of average optical coefficient.

3. Reconstruction Method

3.1. *The two-layered model*

The reconstructive object is to recognize the CO4 part which is different from the other seven parts, shown in Fig. 4. Since the reconstructive model has many parts, the reconstruction is more

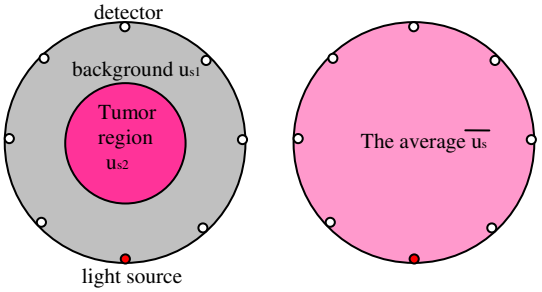

Fig. 2. The simulated models.

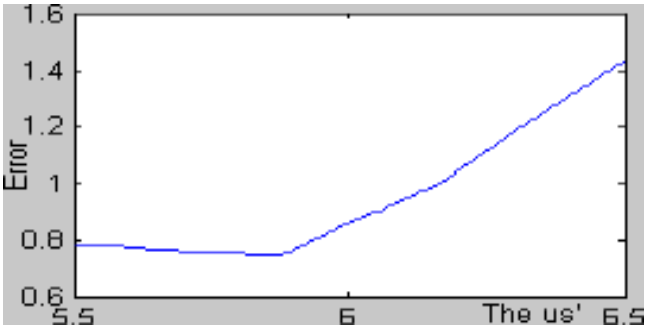

Fig. 3. The error curve of I_1 and I_0, Error $= \sqrt{\Sigma(I_1 - I_0)^2}$.

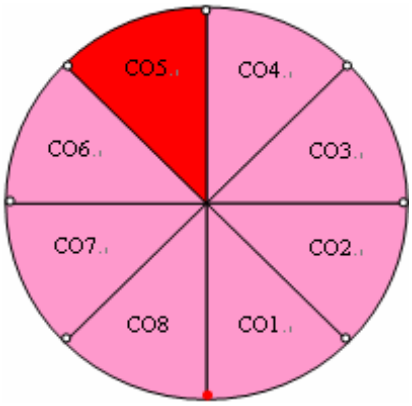

Fig. 4. The reconstructive model.

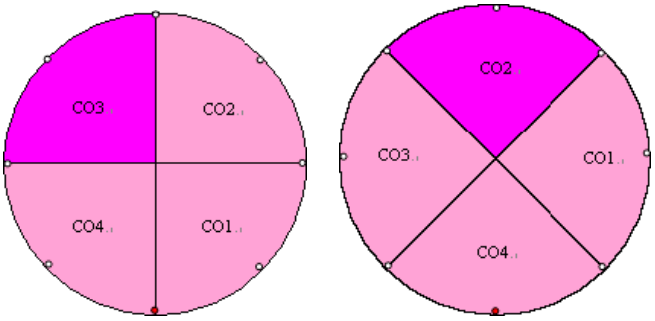

(a) (b)

Fig. 5. The simulated models: (a) Model 1; (b) Model 2.

complex and so the computational speed is slow.[9] In this paper, two simpler models are introduced in Fig. 5. Model 1 is the circle tissue divided into four equal sectors as shown in Fig. 5(a). Model 2 is the sectors rotated 45° as shown in Fig. 5(b). When the μ_s' in part CO4 is different from the other parts in Fig. 4, then it makes part CO2 in Fig. 5 different from other parts, since its $\bar{\mu}_s'$ is different from others. Then according to the definition of the average scattering coefficient, if the same tissue shows different optical properties distribution from the two models simulated, with logic, it is easy to find the tumor part in the reconstructive model.

3.2. *Two-layered BP neural network*

The solution of inverse problem is based on the forward problem, so sample sets of BP neural network can be obtained from the solver of forward problem. The framework of the two-layered BP neural network in the training model is as shown in Fig. 6.

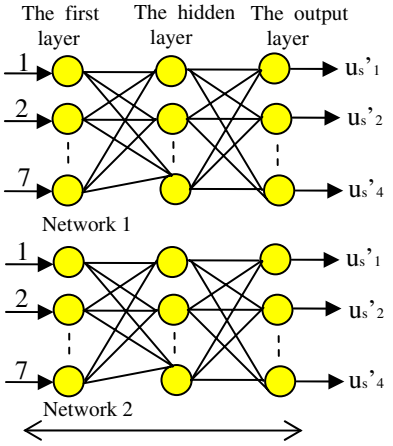

Fig. 6. The framework of the two-layered BP neural network (TLBPNN).

In Fig. 5, μ_{s1}', μ_{s2}', μ_{s3}' and μ_{s4}' are the reduced scattering coefficients of CO1, CO2, CO3 and CO4, respectively. Their values vary from 5 to 15 cm^{-1}. The μ_a is 0.48 cm^{-1} in parts CO1–CO4. The forward method can be used to get the sample set.

3.3. *Optimization algorithm*

The key of inverse problem is to reconstruct optimization algorithm. The Levenberg–Marquardt (LM) algorithm is presented in this paper to train BP network.[10] Training error was shown every 25 times and the network stopped training when $m \leq 1000$ or $e_k \leq 1e-6$.

4. Result and Discussion

4.1. *Reconstruction results*

There are 1331 training samples which are used to train each of the two networks. After adjusting the network parameters and the training conditions, the trained networks can provide optimal results. The test samples are from the reconstruction model shown in Fig. 4. The μ_s' in CO4 is 6, 7, 10, and 15 cm^{-1} (the meaning is the same in the tables whose value is compared with the reconstructive values). The others are 5 cm^{-1} which is the background. Compare the model with Model 1 and 2 shown in Figs. 4 and 5, each part of the sector models corresponds to the two parts in the model. The reconstructive results from the two networks are shown in Tables 1 and 2. There are four cases in the test. It is obvious that μ_{s2}' of the part CO2 in Models 1 and 2 is different from the other parts, which means there is a tumor in it.

Table 1. The μ_s' (cm^{-1}) reconstruction map of the sector network.

μ_s'	$\bar{\mu}_{s1}'$	$\bar{\mu}_{s2}'$	$\bar{\mu}_{s3}'$	$\bar{\mu}_{s4}'$
6	5.0000	5.5358	5.8316	4.7224
7	5.0000	5.8130	5.9681	4.6444
10	5.0000	6.4236	6.2306	4.5187
15	5.0000	6.8451	6.4418	4.4292

Table 2. The μ_s' (cm^{-1}) reconstruction map of the sector rotated 45° network.

μ_s'	$\bar{\mu}_{s1}'$	$\bar{\mu}_{s2}'$	$\bar{\mu}_{s3}'$	$\bar{\mu}_{s4}'$
6	5.0000	6.4380	5.2874	5.1283
7	5.0000	6.7260	5.2507	5.1370
10	5.0000	7.2866	5.2019	5.1434
15	5.0000	7.6990	5.1879	5.1317

Combined with the results of the models, we can conclude that the part CO4 shown in Fig. 4 is different from others.

4.2. *Discussion*

We observe that in Table 1, $\bar{\mu}_{s3}'$ has remarkable changes because the tumor is near the part CO3 and the scattered photon has effects. In Model 1, a portion of the scattered photons are transported into part CO3, which results in the corresponding fiber detector collecting more photons, and then the reconstructive $\bar{\mu}_{s3}'$ is larger than $5\,cm^{-1}$. But in Model 2, the tumor is contained in the part CO2 in which the scattered photons are transported in the other segment, then the influence is much smaller than in Model 1. The other parts can also be discussed with the same reason. Therefore, the distance between the tumor and the around tissue segment decides the reconstructive effort of $\bar{\mu}_{s3}'$ in other parts. Similarly, the effort also depends on the distance from the light source to the tumor. It is obvious that the amount of the photon transported into the tissue near the light source is much more than that far away from the light source.

According to the results reconstructed by the network, it is easy to find the location of the tumor. In order to prove the results, it is reasonable to compare the test samples with the photon intensity collected from the sector models when μ_s' varies from 5 to $15\,cm^{-1}$ in part CO2, others are $5\,cm^{-1}$. The result is shown in Table 3.

When μ_s' is increased, the variable curve of $\bar{\mu}_{s2}'$ in Tables 2 and 3 is shown in Fig. 7. We can see

Table 3. The μ_s' (cm^{-1}) reconstruction map of the sector rotated 45° network.

μ_s'	$\bar{\mu}_{s1}'$	$\bar{\mu}_{s2}'$	$\bar{\mu}_{s3}'$	$\bar{\mu}_{s4}'$
6	5.0000	5.4474	5.0000	5.0000
7	5.0000	5.8043	5.0000	5.0000
10	5.0000	6.5100	5.0000	5.0000
15	5.0000	7.0439	5.0000	5.0000

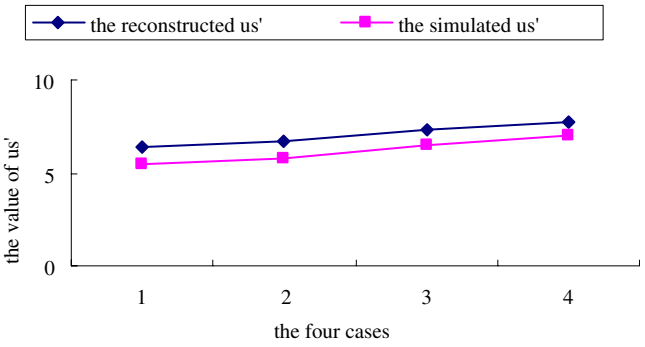

Fig. 7. The trend of the average reduced coefficient.

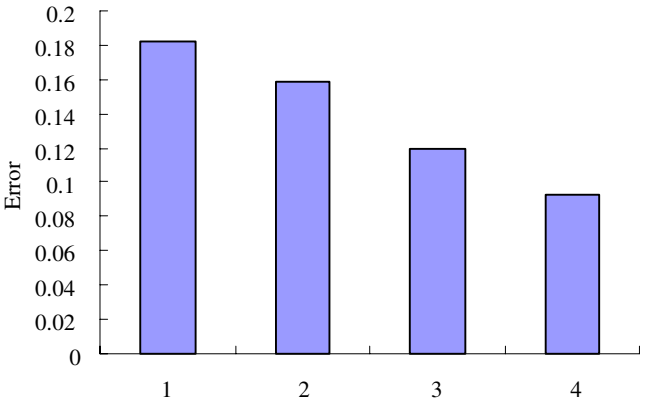

Fig. 8. The error between the reconstructive $\bar{\mu}_{s2}'$ and the simulated μ_s'.

that the trend of two curves is similar; the difference is the size of numerical value which validates the definition of the average optical coefficient. When the tumor tissue is more strongly scattered than the normal tissue, the value of the μ_s' is larger. In this paper, we only studied the data from the sector rotated 45° model. Hence, the reconstructive results are credible. In Fig. 8, $\bar{\mu}_{s2}'$ is larger, the error is smaller. Because the μ_s' in the tumor has obvious difference from the background, the scattering function is strong and the photon intensity is distinct.

5. Conclusion

The primary study of the NIR OT reconstructive technique by two-layered BP neural network was presented in this paper. The inverse problem is solved as optimization problem by the Femlab and Levenberg–Marquardt algorithm. The network can distinguish the location of tumor from the tissue, and the reconstructive μ'_{s2} is not only reasonable but also shows the changes of the transporting photon inside the tissue with tumor. According to above analysis, the influence on the reconstructive effort depends on the distance of the location of the tumor and the light source. In this paper, there is only one fiber transmitting the light. The advantage is the measurement instrument which is very simple, and it is useful for the application of the OT real-time. When the μ'_s in the tumor is close to that around the tissue, the reconstructive error is about 18%. It can be improved by using more fibers transporting the light into the tissue.

The scale of calculation used to train the network can be decreased sharply because the complex model having eight parts was divided into two simple Models 1 and 2 with four parts. Assume that each part needs the scale of calculation N, the reconstructive model with eight parts is N^8, while the model with four parts is N^4, then the two models need $2N^4$. The predominance of the fast method is obvious when the reconstructive tissue is more complex. When the network has been trained, the speed of the reconstructive optical coefficient is only several seconds. It realized the fast reconstruction of tissue optical properties and provided optical OT with a new method.

Future work is needed to reconstruct the model with more parts. Since there is relationship between μ'_s and the temperature of biological tissue, this method will have applications in the temperature measurement and the coagulation of biological tissue.[9]

Acknowledgments

This paper was supported by National Nature Science Foundation of China (Grant No. 30671997). All the work has been done at the Biophotonics Laboratory of NUAA (*www.nuaaphotonics.com*).

References

1. Bluestone, A. Y., Abdoulaev, G., Schmitz, C. H., Barbour, R. L. and Hielscher, A. H., "Three-dimensional optical tomography of hemodynamics in the human head," *Opt. Express* **9**, 272–286 (2001).
2. Nioka. S., Yung, Y., Shnall, M., Zhao, S., Orel, S., Xie, C. *et al.*, "Optical imaging of breast tumor by means of continuous waves," *Adv. Exp. Med. Biol.* **411**, 227–232 (1997).
3. Xu, Y., Iftimia, N., Jiang, H., Key, L. and Bolster, M., *Opt. Exp.* **8**, 447 (2001).
4. Klose, A. D. and Hielscher, A. H., "Optical tomography using the time-independent equation of radiative transfer — Part 2: inverse model," *JQSRT* **72**, 715–732 (2002).
5. Arridge, S. R. and Schweiger, M., "A gradient-based optimization scheme for optical tomography," *Opt. Express* **2**, 213–226 (1998).
6. Meng, J., Wang, J., Huang, X. and Liu, R., "Optical tomography reconstruction based on gradient tree," *J. Quantit. Spectro. Radiat. Transfer* **102**, 181–189 (2006).
7. Qian, Z., Wang, X. and Liu, H., "Study of near infrared guidance technique for 3D targeted localization in neuro-surgery for Parkinson's disease." *Int. Symp. Biophotonics Nanophotonics Metamaterials* **10**, 142–148 (2006).
8. Li, W., Qian, Z. and Wang, H., "Image reconstruction algorithm of near infrared optical tomography," *Chinese Opt. Lett. Supple.* **3**, 237–238 (2005).
9. Li, W. and Qian, Z., "The research on the relationship between the reduced scattering coefficient and temperature of the tissue by NIRS light scattering," *Int. Symp. Biophotonics Nanophotonics Metamaterials* **10**, 162–168 (2006).
10. Wu, Q. and Qian, Z., "An optimization algorithm to inverse problem in 2D optical computed tomography by BP neural network," *Int. Symp. Biophotonics Nanophotonics Metamaterials* **10**, 170–173 (2006).